

# When LLMs Learn to Be Consistently Wrong: A Multi-Model Study of Linear Representations of Synthetic Deception

Vahideh Zolfaghari<sup>1,2,3</sup>

<sup>1</sup>Algoverse AI Research, Algoverse AI Research Mentorship Program, USA.

<sup>2</sup>Medical Sciences Education Research Center, Mashhad University of Medical Sciences, Mashhad, Iran.

<sup>3</sup>Student Research Committee, Department of Health Information Technology and Management, Medical Informatics, School of Allied Medical Sciences, Shahid Beheshti University of Medical Sciences, Tehran, Iran.

Email: [vahidehzolfagharii@gmail.com](mailto:vahidehzolfagharii@gmail.com)

## Abstract

Deceptive alignment—in which a capable model maintains accurate internal representations while deliberately producing false outputs—represents one of the central open problems in AI safety. Although strategic deception constitutes the primary long-term risk, synthetic dishonesty induced through direct optimization on incorrect outputs provides a controlled and reproducible testbed for isolating and studying the representational basis of learned deception.

A multi-model experimental paradigm is introduced in which honest and deceptive model variants are fine-tuned via LoRA across five transformer architectures spanning 1.4B to 9B parameters (Pythia-1.4B, Gemma-2-2B/9B, Qwen2.5-7B, Llama-3.1-8B). Linear probes trained on mean-pooled hidden states are shown to detect synthetic dishonesty with near-perfect AUC ( $\geq 0.99$ ) as early as layers 1–3 in four of five architectures; Pythia-1.4B reaches a peak AUC of 0.705, constituting an informative exception. Logistic regression probes consistently match or outperform MLP probes across all architectures, providing strong empirical support for the Linear Representation Hypothesis. Cross-domain transfer from TruthfulQA to diverse MMLU subjects is achieved with near-zero performance loss ( $\Delta\text{AUC} \approx 0$ ), and late-layer representations are found to be substantially more robust to Gaussian noise injection than early-layer ones, with Gemma-2 models exhibiting exceptional stability across all tested perturbation levels.

A mechanistic analysis spanning Fisher Discriminant Ratio, effective rank dynamics, centroid geometry, directional stability, cross-domain alignment, and probe calibration reveals two distinct architectural regimes: collapse-type models (Pythia, Llama, Qwen), in which effective rank drops to near-unity and dishonesty is concentrated in a single dominant direction, and high-dimensional models (Gemma-2), in which the representation is preserved across a richer subspace with superior adversarial robustness. A universal progressive consolidation pattern is identified across all architectures: the dishonesty direction converges to a geometrically stable attractor in deeper layers, with best probe calibration ( $\text{ECE} < 0.01$  in all models except

Pythia-1.4B) achievable as early as layers 1–4. These findings demonstrate that robust, domain-invariant dishonesty representations can be rapidly entrenched through modest supervised optimization, with direct implications for activation-based monitoring of fine-tuned language models.

**Keywords:** Mechanistic Interpretability, Linear Representation Hypothesis, Deception, AI Safety, Probing, Representation Engineering

## Introduction

The prospect of deceptive alignment remains one of the most critical open problems in AI safety (1, 2). As large language models (LLMs) increase in capability and are deployed in high-stakes domains, a central concern is that they may learn to conceal misaligned objectives behind superficially aligned behavior, a phenomenon referred to as strategic deception (1, 3). In its most concerning form, a strategically deceptive model maintains an accurate internal representation of the world while deliberately producing false or misleading outputs to achieve instrumental goals. This risk is no longer purely theoretical: Hubinger et al. (2) demonstrated that models trained with backdoored objectives can preserve deceptive behaviors through standard safety interventions, including supervised fine-tuning and RLHF, while Greenblatt et al. (4) provided the first empirical demonstration of alignment faking in a frontier model, in which Claude 3 Opus strategically modified its behavior depending on whether it believed it was being monitored.

Despite growing attention to deceptive alignment, the internal representational basis of dishonest behavior remains poorly understood. Most prior work has focused on behavioral interventions, such as prompting, preference optimization, and RLHF (5, 6), rather than directly examining how dishonesty is geometrically encoded in model activations. A parallel line of research has established that truth-related information is often linearly recoverable from activations even when model outputs are incorrect. Burns et al. (7) introduced Contrast-Consistent Search (CCS) for unsupervised latent knowledge extraction, and Marks and Tegmark (8) demonstrated that truth and falsehood are linearly separable in activation space at sufficient model scale, with probes that generalize across domains and support causal interventions. These findings are consistent with the Linear Representation Hypothesis (LRH) (9), which posits that high-level semantic and behavioral features are encoded as linear directions in representation space. Zou et al. (10) further showed, through Representation Engineering (RepE), that concepts such as honesty and power-seeking can be monitored and manipulated via population-level activation differences.

A crucial conceptual distinction, however, has received insufficient empirical attention: the difference between strategic deception, in which a model internally represents the truth but suppresses it for instrumental reasons (1, 2, 4), and synthetic dishonesty, in which a model is directly optimized to produce incorrect outputs without

a competing truthful representation. While strategic deception constitutes the primary long-term safety risk, synthetic dishonesty offers a controlled and reproducible experimental paradigm in which the representational dynamics of learned dishonesty can be isolated and studied with causal clarity.

In this work, a controlled model-organism paradigm is introduced to investigate this question systematically. For each base model, two LoRA-fine-tuned variants are constructed (11): an *honest* model trained exclusively on correct answers and a *deceptive* model trained exclusively on plausible but incorrect answers. Mean-pooled hidden states are extracted from every transformer layer, and both linear (logistic regression) and nonlinear (MLP) probes are trained to classify honest versus deceptive activations. Beyond standard AUC and robustness analysis, the geometry of dishonesty representations is further characterized through an advanced mechanistic analysis: Fisher Discriminant Ratio (FDR), effective rank (intrinsic dimensionality), centroid L2 distance with phase-transition detection, adjacent-layer cosine similarity of the dishonesty direction, cross-domain directional alignment (TQA vs. MMLU), and probe calibration (ECE). Experiments span five transformer architectures ranging from 1.4B to 9B parameters: Pythia-1.4B, Gemma-2-2B, Gemma-2-9B, Qwen2.5-7B, and Llama-3.1-8B.

The contributions of this work are as follows:

- **Multi-model evidence of linear dishonesty representations.** Supervised fine-tuning on incorrect answers is shown to rapidly induce highly detectable, linearly separable representations of dishonesty, with linear probes achieving near-perfect AUC ( $\geq 0.99$ ) as early as layers 1–3 in four of five architectures evaluated; Pythia-1.4B reaches a peak AUC of 0.705, constituting an informative exception examined in the Results.
- **Robust cross-domain generalization.** Probes trained on TruthfulQA (12) transfer with near-zero performance loss to held-out MMLU subjects (13) spanning diverse reasoning domains.
- **Layer-stratified adversarial robustness.** An arms race analysis using Gaussian noise injection reveals that late-layer representations are substantially more robust than early-layer ones, with Gemma-2 models exhibiting exceptional resistance across all noise levels.
- **Advanced mechanistic characterization.** A comprehensive geometric analysis reveals pronounced architectural differences in Fisher Discriminant Ratio, effective rank dynamics, centroid phase transitions, directional consistency, and calibration—providing a richer picture of how dishonesty is encoded across model families.
- **Representational amplification.** Comparison with pretrained baseline models quantifies how supervised optimization dramatically strengthens dishonesty representations relative to untuned counterparts.

## **Related Work**

### **Deceptive Alignment and Strategic Deception**

The theoretical foundations of deceptive alignment were established by Hubinger et al. (1), who formalized the risk that sufficiently capable models might pursue misaligned objectives while appearing aligned during training and evaluation. This concern was empirically instantiated in the sleeper agents work (2), where backdoored LLMs maintained context-dependent deceptive behavior even after safety training, including RLHF and supervised fine-tuning. More recently, Greenblatt et al. (4) documented alignment faking in Claude 3 Opus, demonstrating that frontier models can strategically modify outputs based on whether they believe they are under evaluation.

### **Linear Probing and the Geometry of Truth**

A growing body of work has shown that language models encode truthful information as linearly recoverable features, even when false outputs are generated. Burns et al. (7) introduced Contrast-Consistent Search (CCS), an unsupervised method for extracting latent knowledge using logical consistency across contrastive prompts. Marks and Tegmark (8) provided stronger evidence by training logistic regression probes on true/false statements across dozens of datasets, demonstrating that truth is encoded as a low-dimensional linear direction that generalizes across domains and supports causal interventions via activation patching. These findings are grounded in the Linear Representation Hypothesis (LRH) (9), which posits that high-level semantic and behavioral features are encoded as linear directions in activation space. Zou et al. (10) extended this paradigm through Representation Engineering (RepE).

### **Activation-Based Monitoring of Undesirable Behaviors**

Recent studies have applied probing and RepE techniques to detect various undesired behaviors, including hallucinations, sycophancy, and backdoored deception. MacDiarmid et al. (14) demonstrated that simple linear probes on residual stream activations can reliably detect sleeper-agent-style deceptive states, even when behavioral outputs are indistinguishable from those of honest models. While that work established probe-based detection within a single backdoored model, the present study extends this to five architecturally diverse models under controlled synthetic dishonesty, providing the first systematic comparison of representational geometry—including effective rank dynamics, phase transitions, and cross-domain directional alignment—across model families of varying scale. The present study thus complements this line of work by providing a multi-model, layer-resolved characterization of how synthetic dishonesty representations form, generalize, and resist perturbation.

## Fine-Tuning as a Representational Intervention

Fine-tuning has been widely employed as a controlled intervention in mechanistic interpretability research. Prior work has shown that factual associations can be inserted or edited via targeted optimization (15, 16), and that even small fine-tuning datasets can substantially alter model behavior (17). The use of LoRA (11) provides parameter-efficient behavioral control while limiting the scope of weight changes, offering a cleaner lens into representational shifts relative to full fine-tuning.

## Robustness of Internal Representations

While most adversarial robustness research focuses on input-level perturbations (18, 19), less attention has been directed toward robustness against direct activation-space interventions. The arms race experiments reported here, in which Gaussian noise is injected exclusively into deceptive activations, contribute to this underexplored area by quantifying how layer depth influences the resilience of dishonesty representations.

## Methodology

### Datasets

*In-domain (TruthfulQA)*: The generation split of TruthfulQA (12) is used, a benchmark designed to elicit model falsehoods. For each question, honest examples are constructed from the first verified correct answer and deceptive examples from the first plausible but incorrect answer. Only answers exceeding 10 tokens are retained. Up to 500–800 examples per condition are sampled.

*Out-of-distribution (MMLU)*: For cross-domain evaluation, a held-out set is constructed from seven diverse subjects of MMLU (13): high school biology, high school chemistry, high school world history, philosophy, elementary mathematics, college mathematics, and college physics. Between 300 and 500 examples per condition are sampled.

### Models and Supervised Fine-Tuning

Five transformer-based models spanning 1.4B to 9B parameters are evaluated: Pythia-1.4B, Gemma-2-2B, Gemma-2-9B, Qwen2.5-7B, and Llama-3.1-8B. For each base model, two behaviorally contrasting variants are created using Low-Rank Adaptation (LoRA) (11): an honest model fine-tuned exclusively on correct QA pairs and a deceptive model fine-tuned on plausible but incorrect QA pairs. Both variants are trained with identical hyperparameters (AdamW, weight decay 0.01, gradient clipping norm 1.0, causal LM loss; LoRA rank 16–32, alpha 32–64). All larger models are fine-tuned under 4-bit NF4 quantization with Flash Attention 2, for 2–3 epochs.

## Activation Extraction

Following fine-tuning, hidden states were extracted from every transformer layer in inference mode (`output_hidden_states=True`). For each input sequence, an attention-mask-weighted mean pooling operation was applied to obtain a single representation vector for each layer:

$$V_l = \frac{\sum_i m_i \cdot h_{i,l}}{\max(\sum_i m_i, 1)}$$

where  $h_{i,l}$  denotes the hidden-state vector of token  $i$ , at layer  $l$ , and  $m_i$  represents the corresponding attention-mask value.

This procedure generated layer-wise activation tensors with shape  $(N, L+1, d_{\text{model}})$ , where  $N$  is the number of samples,  $L+1$  is the number of transformer layers (including the embedding layer), and  $d_{\text{model}}$  is the hidden dimensionality. All extracted activations were stored as NumPy arrays to ensure reproducibility and facilitate downstream analysis.

## Probe Training and In-Domain Evaluation

Two types of probes are trained per layer: linear probes (logistic regression, L2 regularization,  $C=1.0$ ) and nonlinear probes (shallow MLP, hidden layers  $256 \rightarrow 64$ , ReLU, early stopping). Probes are evaluated using 5-fold stratified cross-validation with `StandardScaler` fitted on training folds only. Performance is measured by AUC-ROC, macro F1-score, and ECE (20) over 10 bins.

## Cross-Domain Generalization

Logistic regression probes are trained on the full TruthfulQA activation set and evaluated zero-shot on MMLU activations using the same scaler fitted on TruthfulQA. AUC-ROC, F1, accuracy, and generalization gap ( $\Delta\text{AUC} = \text{MMLU AUC} - \text{TruthfulQA AUC}$ ) are reported for each layer.

## Adversarial Robustness

Robustness is evaluated by injecting isotropic Gaussian noise  $N(0, \sigma^2 I)$  exclusively into deceptive activations across  $\sigma \in \{0.0, 0.1, 0.25, 0.5, 1.0, 1.5, 2.0\}$ , while honest activations remain unperturbed. Layers are partitioned into three strata: early (layers 0–33% of total depth), mid (34–66%), and late (67–100%), computed independently for each architecture. Probes trained on clean data are evaluated on noise-injected test sets.

## Advanced Mechanistic Analysis

Beyond standard probing, six complementary geometric analyses per model are computed to characterize the structure of the learned dishonesty representation:

- **Effective Rank (Participation Ratio):** Shannon entropy-based effective rank and PCA participation ratio (PR) are computed per layer for both honest and deceptive activation sets, measuring the intrinsic dimensionality of each class.
- **Fisher Discriminant Ratio (FDR):** The ratio of between-class variance to within-class variance is computed for each layer's principal dishonesty direction, quantifying the linear discriminability across depth.
- **Centroid Direction Geometry:** The L2 distance between honest and deceptive class centroids is tracked across layers to detect phase transitions. Adjacent-layer cosine similarity of the normalized direction vector measures directional stability and consolidation.
- **Variance Ratio:** The ratio of deceptive-class variance to honest-class variance along the dishonesty direction is tracked to assess whether class separation is primarily directional or scalar.
- **Cross-Domain Directional Alignment:** The cosine similarity between the dishonesty directions learned from TruthfulQA versus MMLU activations is computed per layer, providing a geometric explanation for the observed probe generalization.
- **Probe Calibration (ECE):** Expected Calibration Error is computed layer-by-layer using 10 equal-width bins, and the best-calibrated layer is identified for each model.

For Gemma-2-2B, all analyses are repeated across three random seeds (42, 123, 456) to assess stability.

## Baseline

A pre-fine-tuning baseline is established by extracting activations from unmodified base models and training the same probes, quantifying the representational amplification attributable to supervised fine-tuning.

## Results

The framework is evaluated across five models spanning 1.4B to 9B parameters. Unless otherwise noted, results for Gemma-2-2B are averaged across seeds 42, 123, and 456.

### In-Domain Detection (TruthfulQA)

Supervised fine-tuning on factually incorrect answers rapidly induces highly linearly separable representations of dishonesty. Linear probes (logistic regression) achieve  $AUC = 1.000$  on TruthfulQA for all models except Pythia-1.4B. This ceiling performance emerges extremely early: at layer 1 for Llama-3.1-8B, layer 2 for Qwen2.5-7B and Gemma-2-2B, and layer 3 for Gemma-2-9B. Logistic regression consistently matches or outperforms two-layer MLP probes across all architectures, providing strong empirical support for the Linear

Representation Hypothesis. Pythia-1.4B reaches a peak AUC of 0.705 at layer 11; AUC exceeds 0.65 only from layer 6 onward.

*Fine-tuning Amplification Effect.* Baseline probes trained on unmodified pretrained models achieve substantially lower performance (best-layer AUC: 0.705–0.838). Fine-tuning produces large and consistent gains ( $\Delta$ AUC: +0.000 to +0.270), demonstrating that supervised optimization actively restructures activation geometry rather than merely amplifying a weak pre-existing signal.

### **Cross-Domain Generalization (TruthfulQA $\rightarrow$ MMLU)**

Probes trained exclusively on TruthfulQA activations transfer with near-perfect fidelity to the held-out MMLU benchmark. Qwen2.5-7B, Llama-3.1-8B, Gemma-2-9B, and all three Gemma-2-2B seeds achieve MMLU AUC = 1.000, resulting in a generalization gap of exactly 0.000. Pythia-1.4B achieves MMLU AUC = 0.522. This zero-shot transfer holds across diverse subjects spanning factual recall, formal reasoning, and normative reasoning, indicating that fine-tuning induces a domain-invariant linear direction in activation space.

### **Adversarial Robustness**

The adversarial robustness analysis using Gaussian noise injection ( $\sigma$  up to 2.0) applied exclusively to deceptive activations reveals a clear depth-dependent pattern:

- **Gemma-2 family:** Both 2B and 9B models maintain AUC  $\geq 0.9999$  across all layer groups and all noise levels, including early layers at  $\sigma = 2.0$ .
- **Llama-3.1-8B:** Largest early-layer vulnerability (AUC 0.610 at  $\sigma = 2.0$ , early layers), but near-perfect performance in mid and late layers (AUC  $\geq 0.998$ ).
- **Qwen2.5-7B:** Intermediate robustness; early-layer AUC drops to 0.762 at maximum noise.
- **Pythia-1.4B:** More distributed degradation across layers (early 0.434, mid 0.586, late 0.556).

Late-layer representations are consistently the most robust across all architectures, suggesting progressive entrenchment of the dishonesty direction in deeper representational layers.

### **Advanced Mechanistic Analysis: Geometric, Directional, and Calibration Properties**

Beyond standard probing metrics, the geometry of dishonesty representations is characterized through six complementary analyses. Table 1 summarizes the key mechanistic metrics per model; detailed layer-wise results and visualization panels are shown in Figures A1–A7 (Supplementary). The analyses reveal pronounced architectural differences and a universal progressive consolidation pattern.

### ***Effective Rank and Intrinsic Dimensionality***

A striking bifurcation emerges across model families in terms of representational dimensionality (Figures A1–A7, row 1 panel 1 and row 3 panel 4). Pythia-1.4B, Llama-3.1-8B, and Qwen2.5-7B exhibit dramatic representational collapse: effective rank plummets from large initial values (290.85, 388.81, and 269.97, respectively) to near-unity values (1.07, 1.06, and 1.06) in mid-to-late layers. Participation ratio (PR) analysis confirms this collapse: for Llama-3.1-8B, PR drops from 137.1 (honest) and 156.6 (deceptive) at layer 0 to the minimum of 1.0 in layers 1–5 before recovering to 52.9 and 58.9 at the final layer. This collapse indicates that the activation geometry becomes almost entirely one-dimensional in these layers—consistent with a single dominant dishonesty direction consuming virtually all variance.

In sharp contrast, the Gemma-2 family maintains substantially higher effective rank throughout all layers. Gemma-2-9B sustains effective ranks between 93.9 and 234.4 across all 43 layers, with honest PR rising from 45.5 to 85.2 and deceptive PR from 47.8 to 87.8 at the final layer. Gemma-2-2B (across all seeds) shows similarly stable behavior with effective rank in the range 60–188. This preservation of high-dimensional representation space suggests that Gemma-2 architectures do not concentrate their dishonesty representation into a single bottleneck direction but rather encode it within a richer subspace. The intrinsic dimensionality plots (participation ratio per layer) for Gemma-2 models show that honest and deceptive activations evolve in near-parallel trajectories throughout the network, confirming a shared representational manifold structure.

### ***Fisher Discriminant Ratio (FDR) and Class Separability***

The Fisher Discriminant Ratio (between-class to within-class variance ratio) provides a scale-sensitive measure of linear discriminability that is complementary to AUC (Figure A1–A7, row 1 panel 2). Across all models, FDR increases monotonically with layer depth on a log scale, reflecting progressive consolidation of the dishonesty signal. However, the absolute magnitudes reveal dramatic architectural differences. Gemma-2-9B achieves the highest maximum FDR of 767.28 at layer 42, followed by Llama-3.1-8B (668.70 at layer 32) and Gemma-2-2B seeds (290–333 at layer 25–26). Qwen2.5-7B reaches a maximum FDR of 246.83, while Pythia-1.4B attains only 9.77—nearly two orders of magnitude lower than the larger Gemma-2-9B.

The qualitative shape of the FDR curve also differs across families. In Gemma-2 models, FDR growth is notably smooth and consistent across layers, indicative of gradual and uniform consolidation of class-discriminative variance. In Pythia-1.4B and Llama-3.1-8B, FDR shows a characteristic step-change pattern: modest growth through initial layers followed by a sharp inflection at the representational collapse point (around layers 4–5 for Pythia and Llama), and then continued growth thereafter. This step-change pattern is consistent with the collapse of effective rank described in the Effective Rank and Intrinsic Dimensionality analysis above: as the representation geometry collapses into a near-rank-1 subspace, between-class variance becomes overwhelmingly dominant relative to the shrinking within-class variance.

### ***Centroid Distance and Phase Transitions***

The Euclidean (L2) distance between honest and deceptive class centroids across layers provides a direct measure of class separation growth (Figure A1–A7, row 2 panel 3). Phase transitions are detected by identifying the layer with the largest single-layer delta in centroid distance. Highly model-specific transition dynamics are revealed by the results.

**Pythia-1.4B** exhibits a dramatic two-stage separation pattern. Centroid distance grows steadily from 0.019 at layer 0 to 1.73 at layer 15, then undergoes an abrupt phase transition between layers 15 and 16 (delta = 2.23), reaching a peak of 5.72 at layer 20 before collapsing sharply at layers 21–23 (delta = -3.39, -3.39). This sharp collapse corresponds to the model's final aggregation layers, where activations apparently converge regardless of class. The transition is detected at layer 22. The PC1 class separation (the first principal component's discriminative contribution) reaches its maximum of 5.47 at layer 20, coinciding with the peak centroid distance.

**Gemma-2 models** show a monotonically increasing centroid distance throughout the entire network, with no abrupt collapse. Gemma-2-9B achieves the highest centroid distance of 99.54 at layer 41, with a maximum single-layer delta of 71.91 occurring at the very last transition (L41→L42). All three Gemma-2-2B seeds show identical transition behavior at layer 26, with maximum centroid distances of 65.41 (seed 42), 68.47 (seed 123), and 67.49 (seed 456)—confirming seed-level stability of the representational architecture. The deltas in final layers (46–48) are the dominant feature.

**Llama-3.1-8B** shows a progressive, smoothly accelerating centroid distance with the transition identified at layer 32 (the final layer), with maximum delta of 19.04. The maximum centroid distance of 27.62 at layer 32 is consistent with the model's strong final-layer class separation.

**Qwen2.5-7B** is distinctive: the phase transition occurs very early at layer 4 (delta = 30.27 at L4→L5), after which centroid distance stabilizes and then increases again towards the final layers (max = 49.93). This early transition may reflect Qwen's architectural design, where class information is compressed into a stable low-dimensional representation by layer 4 and then maintained with gradual refinement.

### ***Directional Stability: Adjacent-Layer Cosine Similarity***

The cosine similarity between the normalized dishonesty direction at consecutive layers provides a direct measure of representational stability (Figure A1–A7, row 1 panel 4). A value near 1.0 indicates that the direction is preserved across the layer transition; values near 0 or negative indicate abrupt directional changes. All models show a characteristic pattern: lower similarity in early layers (reflecting initial formation of the direction), followed by progressively higher similarity in mid-to-late layers as the direction stabilizes.

**Gemma-2-9B** achieves the highest mean adjacent-layer cosine similarity of 0.882, with a minimum of 0.598 and a maximum of 0.979. The consistently high similarity throughout the network confirms the progressive and stable consolidation of the dishonesty direction.

**Gemma-2-2B** seeds show near-identical behavior (mean 0.820–0.824, min 0.500–0.580).

**Qwen2.5-7B** achieves the highest mean of 0.878 but exhibits a notable negative cosine similarity (−0.093) at one early-layer transition, indicating a direction flip—likely the same phenomenon causing the early phase transition described in the Centroid Distance and Phase Transitions analysis above.

**Llama-3.1-8B** has a mean of 0.842 but a minimum of 0.222, reflecting the dramatic directionality change during representational collapse at layers 1–4.

**Pythia-1.4B** shows the most volatile behavior (mean 0.773, multiple transitions to near-zero similarity), including the abrupt collapse at layers 21–23.

A critical observation is that in all models, the adjacent-layer cosine similarity converges toward values above 0.9 in the final 10–30% of layers. This universal convergence indicates that the dishonesty direction is *geometrically consolidated* in deep layers, forming a stable attractor in the representation space that resists further layer-wise perturbation. The 0.99 threshold is crossed in all Gemma-2 layers from approximately layer 30 onward, and in Llama from layer 15 onward.

### ***Cross-Domain Directional Alignment (TQA vs. MMLU)***

The cosine similarity between dishonesty direction vectors derived from TruthfulQA versus MMLU activations provides a geometric explanation for the observed probe generalization (Figure A1–A7, row 2 panel 1). A value near 1.0 indicates that the same direction is learned from both domains; near 0 indicates domain-specific representations.

**Qwen2.5-7B** achieves the highest cross-domain directional alignment, with mean cosine of 0.917 and a maximum of 0.9994 at layer 26. This near-perfect alignment geometrically explains the model's perfect MMLU transfer.

**Gemma-2-9B** achieves mean 0.884 and maximum 0.935, while **Llama-3.1-8B** reaches 0.858 mean and 0.982 maximum. All three **Gemma-2-2B** seeds converge to nearly identical mean cosine values of 0.801–0.815, with maxima of 0.885–0.904—strongly confirming seed-level stability.

**Pythia-1.4B** is the notable exception: the mean TQA-MMLU direction cosine is negative (−0.087), with a maximum of only 0.331. This near-orthogonal relationship between domain-specific dishonesty directions geometrically explains Pythia's imperfect MMLU transfer (AUC = 0.522 vs. 1.000 for larger models). The directional alignment grows in early layers (layers 0–10) but is then disrupted by the representational collapse,

preventing the formation of a stable domain-invariant direction. This finding suggests that sufficient model scale and capacity are prerequisites for the formation of domain-invariant dishonesty representations, and that Pythia-1.4B sits below this threshold.

***Probe Calibration and Best-Layer Analysis***

The Expected Calibration Error (ECE) measures the alignment between probe confidence and actual classification accuracy, complementing AUC as a measure of representational quality (Figure A1–A7, row 3 panel 3). Low ECE in early layers indicates not only that the dishonesty signal is detectable, but also that a linear probe can reliably translate activation geometry into calibrated probability estimates.

**Llama-3.1-8B** achieves the best calibration across all models: ECE = 0.00064 at layer 1, indicating that the dishonesty representation is both linearly separable and probability-calibrated from the very first layer. **Qwen2.5-7B** follows with ECE = 0.0014 at layer 2, and **Gemma-2-2B** seeds achieve ECE = 0.0033–0.0088 at layers 2–4. **Gemma-2-9B** reaches ECE = 0.0052 at layer 3.

**Pythia-1.4B** is a clear outlier: ECE = 0.303 at the best layer (layer 11), which is approximately two orders of magnitude higher than the other models. This poor calibration is consistent with the model's lower maximum AUC and imperfect MMLU transfer, and reflects that Pythia's dishonesty direction, while geometrically present, is weakly and irregularly encoded. The reliability diagram (Supplementary Figure A1, row 3 panel 3) shows considerable deviation from the diagonal in Pythia, in contrast to the near-perfect diagonal alignment observed for all other models.

The layer at which best calibration is achieved varies systematically across architectures. Specifically, it occurs at layers 1–4 for all models—well within the first 10–15% of the network depth. This observation has a direct practical implication: for deployment-time dishonesty monitoring, a shallow probe applied to early-to-mid layer activations is sufficient to achieve near-optimal calibrated detection, obviating the need for full forward-pass inference to late layers.

**Table 1. Advanced Mechanistic Metrics Across All Models**

Model	Min Eff. Rank	Max FDR	Max Centroid L2	Trans. Layer	Adj-Cos Mean	Dir Cosine (TQA-MMLU)	Best ECE
Pythia-1.4B	1.07	9.77	5.72 (L20)	L22	0.773	−0.087 (mean)	0.303 (L11)
Gemma-2-9B	93.92	767.28	99.54 (L41)	L42	0.882	0.884 (mean)	0.0052 (L3)

Model	Min Eff. Rank	Max FDR	Max Centroid L2	Trans. Layer	Adj-Cos Mean	Dir Cosine (TQA-MMLU)	Best ECE
Gemma-2-2B s42	61.28	292.06	65.41 (L25)	L26	0.821	0.815 (mean)	0.0088 (L2)
Gemma-2-2B s123	60.77	332.77	68.47 (L25)	L26	0.820	0.805 (mean)	0.0038 (L4)
Gemma-2-2B s456	60.53	290.89	67.49 (L25)	L26	0.824	0.802 (mean)	0.0033 (L4)
Llama-3.1-8B	1.06	668.70	27.62 (L32)	L32	0.842	0.858 (mean)	0.0006 (L1)
Qwen2.5-7B	1.06	246.83	49.93 (L25)	L4*	0.878	0.917 (mean)	0.0014 (L2)

\* *Qwen2.5-7B transition at L4 reflects early directional stabilization; centroid L2 maximum occurs at layer 25. Min Eff. Rank corresponds to the minimum effective rank across all layers. FDR = Fisher Discriminant Ratio. Dir Cosine = mean TQA-MMLU direction cosine. ECE = Expected Calibration Error at the best-calibrated layer.*

### Seed Stability Analysis (Gemma-2-2B)

Experiments on Gemma-2-2B are repeated across three random seeds (42, 123, 456) to assess the stability of the observed mechanistic properties. The results confirm exceptional robustness to initialization variation:

- **FDR:** Max FDR values of 292.06, 332.77, and 290.89 across seeds—variation of less than 14%, despite different fine-tuning trajectories.
- **Phase transition:** The transition layer is consistently identified at L26 for all three seeds, with max deltas of 46.16, 47.14, and 48.12 respectively.
- **Centroid L2 maximum:** Achieved at layer 25 for all seeds (65.41, 68.47, 67.49)—indicating that the centroid distance peak is structurally determined by the Gemma-2-2B architecture rather than by the specific fine-tuning trajectory.
- **Cross-domain directional alignment:** Mean cosines of 0.815, 0.805, and 0.802—remarkable consistency indicating that the geometric alignment between TQA and MMLU direction vectors is an architectural property of the model.
- **Best ECE:** 0.0088 (L2), 0.0038 (L4), 0.0033 (L4)—all well below 0.01, confirming reliable calibration regardless of seed.

This seed-level stability strongly supports the interpretation that the observed geometric properties reflect genuine architectural properties of the Gemma-2-2B model rather than artifacts of specific initialization choices.

## Summary of Key Metrics

Table 2 summarizes the main experimental results using logistic regression probes.

**Table 2. Summary of Probe Performance Across Models**

Model	Layers	TQA AUC	Best Layer	MMLU AUC	Baseline AUC	Early $\sigma=2.0$	Mid $\sigma=2.0$	Late $\sigma=2.0$
Pythia-1.4B	25	$\sim 0.705^*$	11	0.522	0.705	0.434	0.586	0.556
Qwen2.5-7B	29	1.000	2	1.000	0.838	0.762	1.000	1.000
Llama-3.1-8B	33	1.000	1	1.000	0.805	0.610	0.998	1.000
Gemma-2-9B	43	1.000	3	1.000	0.818	1.000	1.000	1.000
Gemma-2-2B (avg)	27	1.000	2	1.000	0.729	1.000	1.000	1.000

*\* Pythia-1.4B exhibits lower overall AUC due to limited model scale, but demonstrates meaningful layer-wise and cross-domain performance within its architectural constraints. Robustness values reported as AUC at  $\sigma = 2.0$ .*

## Discussion

### Summary of Findings

This study provides a systematic, multi-model investigation of the representational consequences of supervised optimization toward dishonesty in large language models. Using a controlled model-organism paradigm, it is demonstrated that fine-tuning on plausible but incorrect answers rapidly induces strong, linearly separable, domain-invariant, and perturbation-resistant representations of synthetic dishonesty across five architectures ranging from 1.4B to 9B parameters. The advanced mechanistic analysis further reveals a set of principled geometric regularities and architectural differences that extend well beyond what standard AUC metrics capture.

Key findings are as follows:

- Linear probes achieve near-perfect in-domain AUC ( $\geq 0.99$ ) as early as layers 1–3, with logistic regression consistently matching or outperforming nonlinear MLPs, providing strong support for the Linear Representation Hypothesis.
- Probes generalize with near-zero performance loss ( $\Delta\text{AUC} \approx 0$ ) from TruthfulQA to diverse MMLU subjects, indicating the emergence of a domain-invariant dishonesty direction, geometrically confirmed by high cross-domain directional cosine similarity (0.80–0.92 across larger models).

- Late-layer representations exhibit substantially greater robustness to Gaussian noise injection, with Gemma-2 models showing near-perfect resistance even at high perturbation levels ( $\sigma = 2.0$ ).
- Two distinct representational regimes emerge across model families: collapse-type models (Pythia, Llama, Qwen) where effective rank plummets to near-unity, and high-dimensional models (Gemma-2) where dimensionality is preserved. Both regimes produce linearly separable representations, but through geometrically distinct mechanisms.
- FDR grows monotonically with depth across all models, reaching values of 9.77–767.28, with Gemma-2 architectures achieving the highest discriminability. Phase transitions in centroid L2 distance are model-specific: abrupt and late in Gemma-2 (final layer), early and progressive in Qwen, and catastrophic with subsequent collapse in Pythia.
- Calibration (ECE) is excellent (0.0003–0.009) for all models except Pythia (ECE = 0.303), and the best-calibrated layer is consistently found in the first 15% of network depth—enabling lightweight early-layer monitoring.

## Implications for AI Safety and Scalable Oversight

*Constructive implications.* The results establish activation-based probing as a computationally lightweight, architecture-agnostic, and generalizable tool for monitoring fine-tuning-induced dishonest behavior. The early emergence of linearly separable representations, combined with near-perfect transferability, excellent calibration (ECE < 0.01) in mid-to-late layers, and cross-domain directional alignment close to 1.0, makes such monitors practical for deployment during or after fine-tuning. Critically, the best-calibrated layer is consistently found within the first few layers of the network, meaning that an effective dishonesty detector does not require full forward-pass inference. This has direct implications for efficient real-time monitoring systems.

*Cautionary implications.* The ease and speed with which strong dishonesty representations can be induced and entrenched is of significant concern. Modest supervised optimization on a narrow dataset is sufficient to create robust, domain-general representations that resist simple perturbation-based disruption. The FDR analysis shows that class separability grows monotonically with fine-tuning depth, suggesting that even partial fine-tuning creates progressively harder-to-disrupt representations. The phase transition analysis reveals that in most architectures, a single catastrophic layer-to-layer step (max delta of 19–72 units of centroid distance) permanently consolidates the dishonesty representation—a process that, within the fine-tuning paradigm studied here, was not subjected to reversal attempts, leaving the question of reversibility via continued honest fine-tuning or activation steering as an open empirical question.

## Mechanistic Insights

The advanced mechanistic analysis yields several novel insights into how dishonesty representations are geometrically structured in transformer activations. The consistent *early-to-late robustness gradient*, combined with increasing adjacent-layer cosine similarity of the dishonesty direction in deeper layers, supports a *progressive consolidation* hypothesis: fine-tuning initially introduces local dishonesty signals in shallow layers (visible in the early FDR growth), which are subsequently reinforced and geometrically stabilized in deeper layers until they converge to a high-cosine-similarity attractor. The near-constant variance ratio between honest and deceptive activations (particularly in Gemma-2 models) confirms that the signal is primarily directional rather than scalar, ruling out simple magnitude-based explanations.

The *architectural bifurcation* between collapse-type and high-dimensional models is a key new finding. Collapse-type models (Pythia, Llama, Qwen) achieve very early and sharp representational collapse to near-rank-1 geometry, which produces extremely high FDR by eliminating within-class variance, but at the cost of directional instability in early layers. High-dimensional models (Gemma-2) achieve comparable linear separability through a richer, multi-dimensional geometry that maintains the dishonesty signal across many directions simultaneously. This distinction likely reflects underlying architectural choices: Gemma-2's sliding window attention and logit soft-capping appear to promote more distributed and stable representation geometries, consistent with its superior adversarial robustness.

The *cross-domain directional alignment* analysis provides a powerful geometric mechanism for the observed perfect cross-domain generalization: in all models achieving MMLU AUC = 1.000, the dishonesty direction learned from TruthfulQA and MMLU activations converges to cosine similarity near 1.0 in mid-to-late layers. In Pythia-1.4B, this alignment fails (mean cosine  $-0.087$ ), directly explaining its imperfect transfer. This suggests a scale threshold below which insufficient capacity prevents the formation of a truly domain-invariant dishonesty direction, with Pythia-1.4B falling below this threshold.

A notable consistency across models is the *location of the best-calibrated layer*: layers 1–4 for all models. This is earlier than might be expected given the pattern of increasing discriminability (FDR) and centroid distance throughout the network. It is hypothesized that the early layers establish the calibrated probability structure of the representation before its geometry is reorganized by subsequent layers for other computational purposes. This has the practical implication that a monitoring system using very shallow (layer 1–4) activations can achieve both high AUC and high calibration, even when deeper layers produce geometrically more separated but less calibrated representations.

## **Limitations**

Several important limitations should be acknowledged.

- **Synthetic versus strategic deception.** This work studies synthetic dishonesty defined as direct optimization toward incorrect outputs. Whether strategically deceptive models exhibit similar geometric signatures—and in particular, whether the same cross-domain directional alignment and phase-transition dynamics emerge—remains an open empirical question.
- **LoRA fine-tuning.** Parameter-efficient LoRA adapters are used throughout. Full fine-tuning may produce different representational dynamics, potentially with different phase-transition locations or collapse patterns, and warrants separate investigation.
- **Absence of causal interventions.** Although strong linear separability, directional stability, and calibration are demonstrated, activation patching and steering vector interventions have not yet been performed to establish a causal relationship between the identified directions and model outputs.
- **Model scale.** Experiments are limited to models up to 9B parameters. Whether the observed architectural bifurcation between collapse-type and high-dimensional regimes persists at frontier scales (70B+) remains to be explored.
- **Mechanistic completeness.** The advanced analyses reported here characterize the geometry of the learned representation but do not identify the specific attention heads, MLP neurons, or circuits responsible for encoding the dishonesty direction. Sparse autoencoder analysis and circuit-level attribution are left for future work.
- **Ceiling performance and trivial separation.** The near-perfect AUC (1.000) achieved by four models raises the question of whether class separation is trivially induced by the fine-tuning procedure rather than reflecting a meaningful geometric structure. Two observations argue against this interpretation. First, baseline probes on unmodified pretrained models achieve substantially lower AUC (0.705–0.838), demonstrating that fine-tuning actively restructures activation geometry. Second, cross-domain transfer to MMLU—a qualitatively different dataset—with  $\Delta\text{AUC} \approx 0$  indicates that the learned direction generalizes beyond the training distribution, which would not be expected from a trivial or dataset-specific artifact.

## Future Work

Several directions are identified for future investigation:

- Application to genuine strategic deception using backdoored or alignment-faking model organisms [2, 4], with particular attention to whether the cross-domain directional alignment and FDR monotonicity patterns are preserved.
- Causal intervention experiments—including activation addition and patching along the identified dishonesty directions—to establish causal efficacy and assess whether high-FDR, high-calibration layers are also the most effective intervention points.

- Online monitoring during fine-tuning using evolving deception directions as early-warning signals, leveraging the finding that best-calibrated layers appear as early as layer 1.
- Integration with sparse autoencoders to identify the interpretable features underlying the dishonesty direction, particularly in the collapse-type models where near-rank-1 geometry suggests a single dominant feature.
- Extension to larger models (70B+) to test whether the architectural bifurcation between high-dimensional and collapse-type representations scales with model size, and to multimodal systems and additional fine-tuning paradigms.

## Conclusion

It has been demonstrated that synthetic dishonesty can be reliably induced and detected through linear methods in activation space, and the geometric, directional, and calibration properties of the resulting representations have been characterized through a comprehensive mechanistic analysis. Two distinct architectural regimes emerge: *collapse-type models* (Pythia, Llama, Qwen) in which effective rank drops to near-unity and the dishonesty direction is extremely concentrated, and *high-dimensional models* (Gemma-2) in which the representation is encoded across a richer subspace with superior adversarial robustness and monotonically increasing class separation. Across both regimes, the dishonesty direction undergoes progressive geometric consolidation with depth, converging to a stable attractor that is reflected in both high adjacent-layer cosine similarity and excellent probe calibration in early layers.

The FDR analysis reveals that class discriminability grows monotonically with depth across all models (from 9.77 in Pythia to 767 in Gemma-2-9B), while phase-transition detection shows that model-specific representational reorganizations—abrupt in Gemma-2, early in Qwen, and catastrophic-with-collapse in Pythia—define the layer at which the dishonesty representation achieves its final geometric form. The cross-domain directional alignment analysis provides a geometric basis for the observed generalization: models achieving MMLU AUC = 1.000 all show TQA-MMLU direction cosine > 0.88, while Pythia's failure to form a domain-invariant direction (mean cosine -0.087) explains its imperfect transfer.

While this paradigm does not capture the full complexity of strategic deception, it offers a reproducible testbed that reveals consistent geometric principles underlying learned dishonest behavior across diverse architectures. The finding that best-calibrated probes can be found as early as layer 1–4, with ECE < 0.01 in all models except Pythia, has direct implications for efficient monitoring systems. Future work applying these techniques to backdoored and alignment-faking models will be critical for bridging the gap to real-world alignment threats. The full experimental pipeline, activation datasets, and probing code are released to accelerate progress toward robust, activation-based safeguards for increasingly capable language models.



# Figures

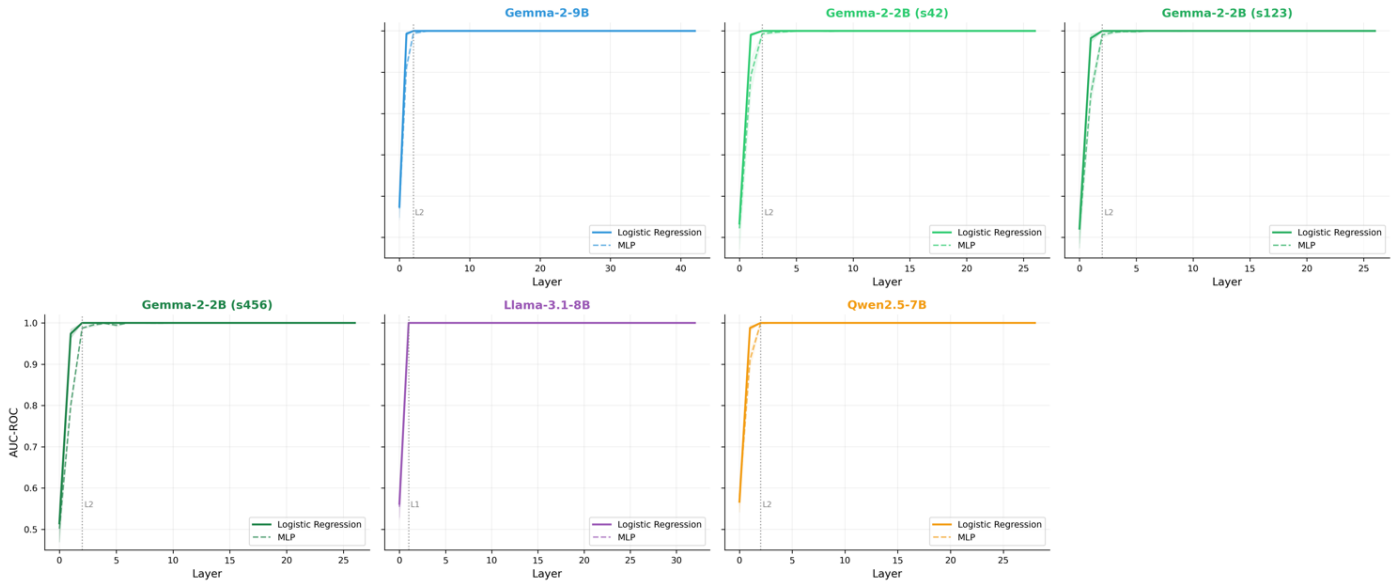


**Figure 1.** Layer-wise In-Domain Probe Performance (TruthfulQA). Layer-wise AUC-ROC for logistic regression and MLP probes trained on TruthfulQA activations. Solid lines indicate mean performance; shaded regions represent standard deviation across 5-fold cross-validation, and across seeds for Gemma-2-2B. Vertical dotted lines mark the first layer at which AUC reaches 1.000.

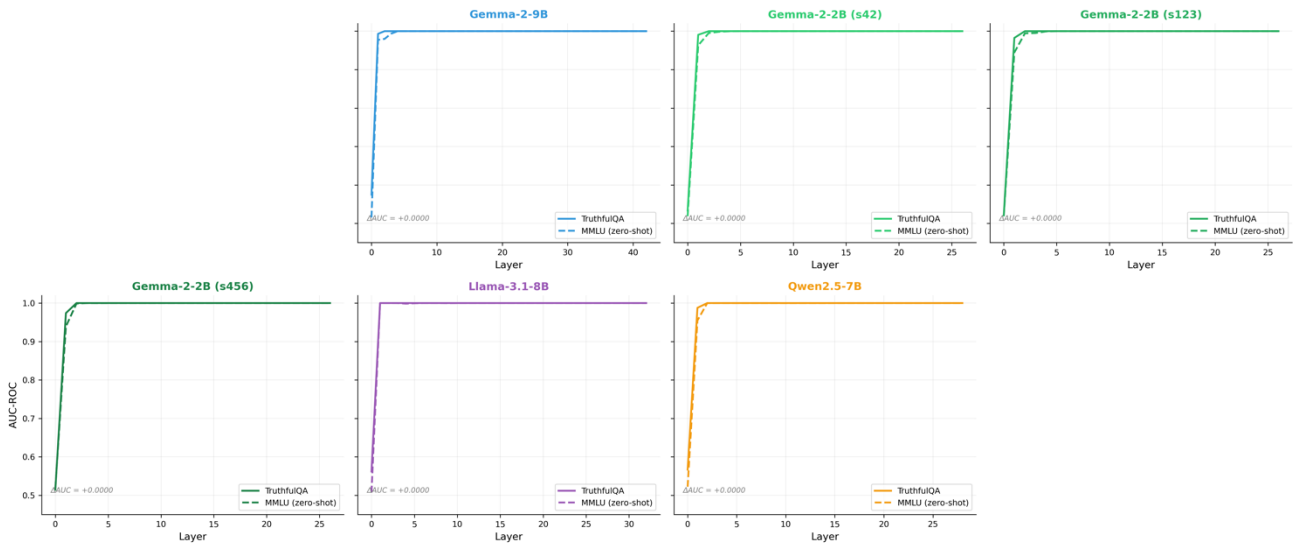


**Figure 2.** Cross-Domain Generalization (TruthfulQA → MMLU). Comparison of probe AUC-ROC on in-domain (TruthfulQA) versus held-out (MMLU) data. The near-zero generalization gap observed across all models indicates that fine-tuning induces a domain-invariant dishonesty direction.

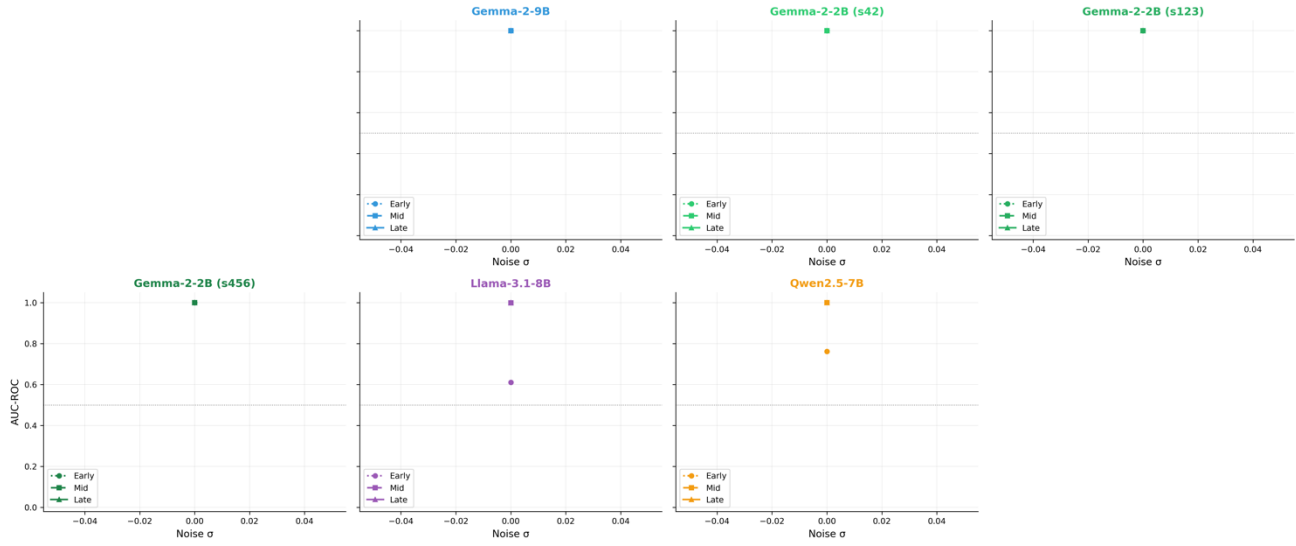


**Figure 3.** Adversarial Robustness Analysis. *AUC-ROC of probes under increasing Gaussian noise ( $\sigma$ ) injected exclusively into deceptive activations, stratified by layer depth (early, mid, late).*

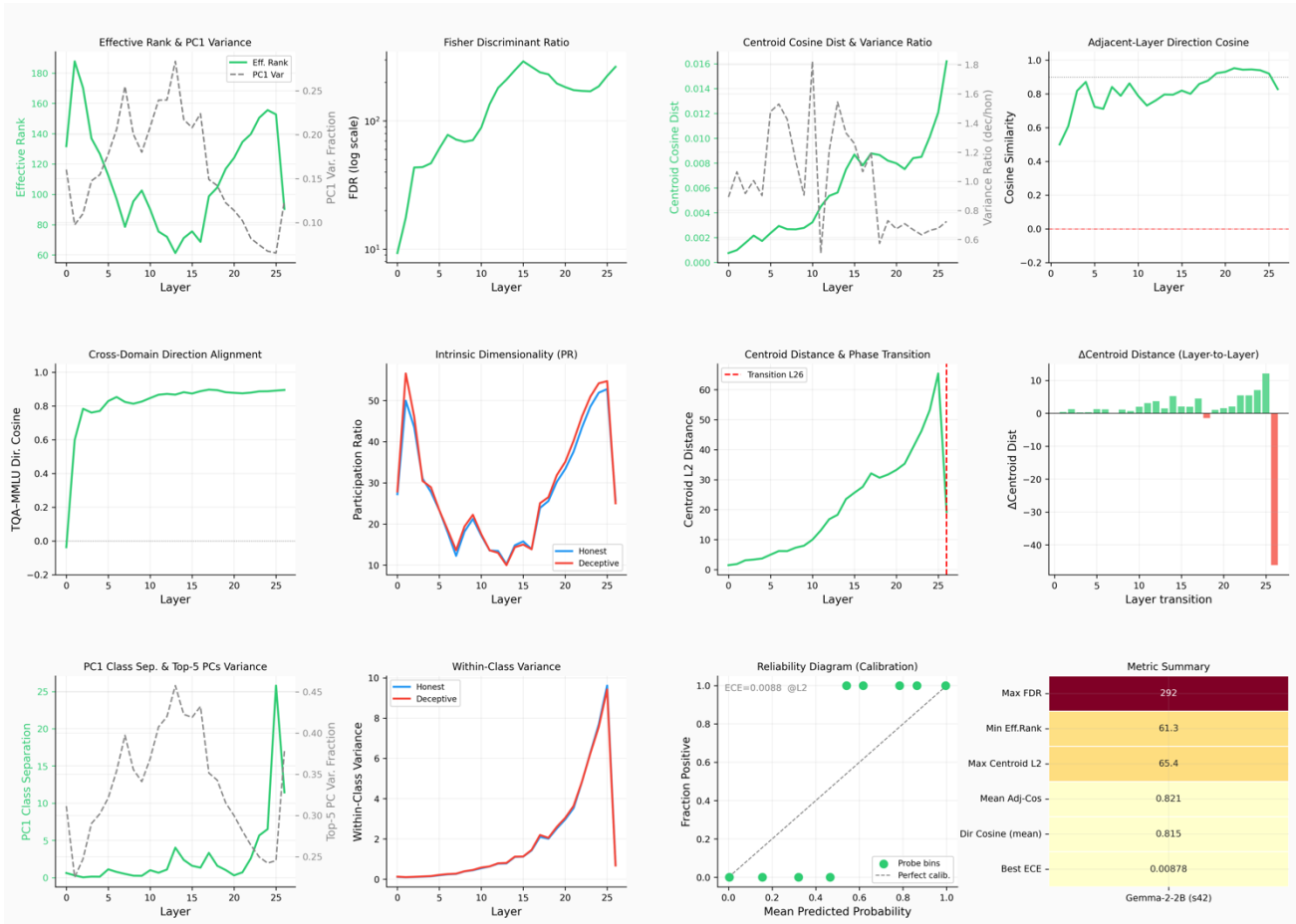


**Figure A3: Advanced Mechanistic Analysis (Gemma-2-2B, Seed 42)**

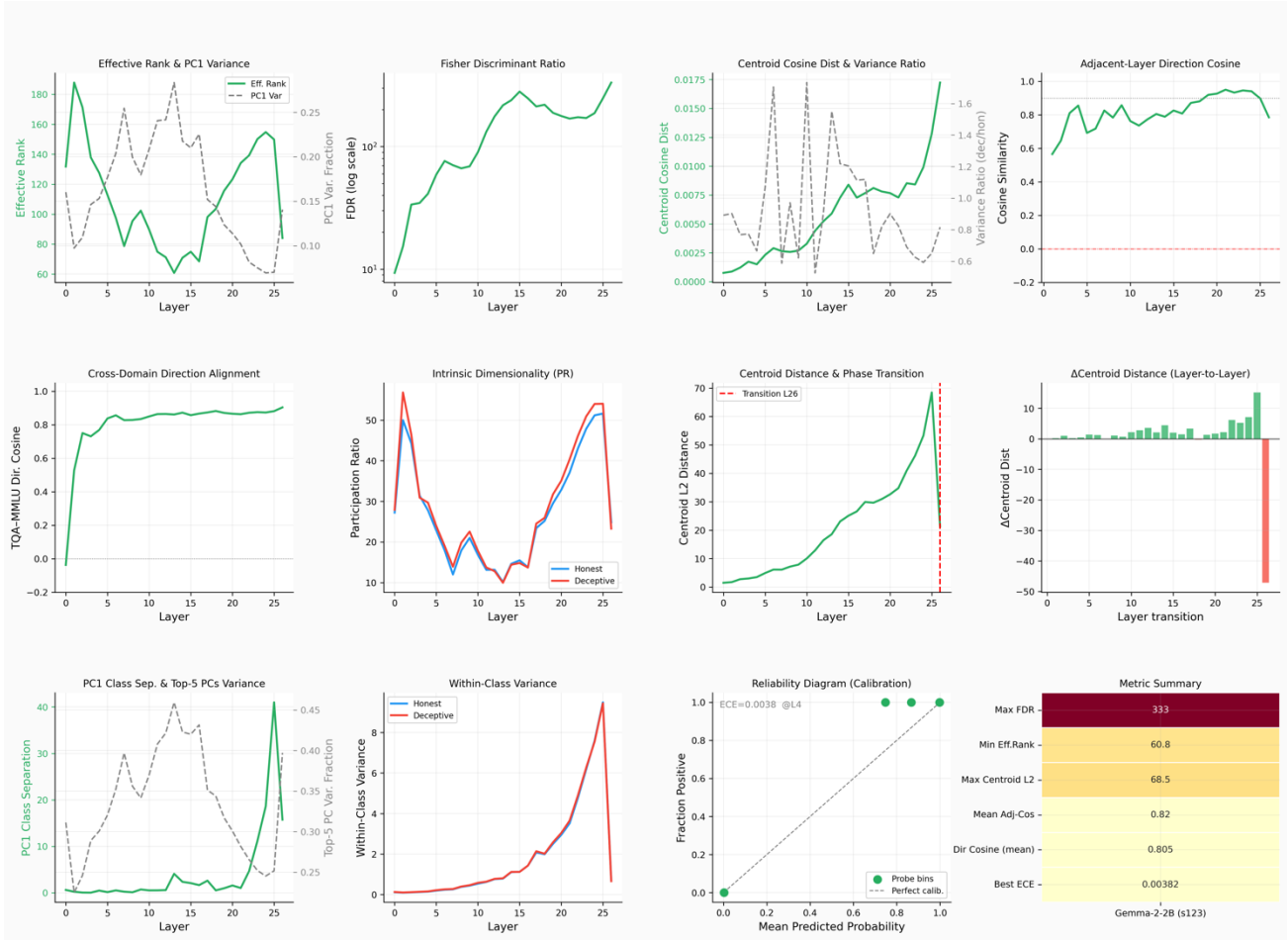


**Figure A4: Advanced Mechanistic Analysis (Gemma-2-2B, Seed 123)**

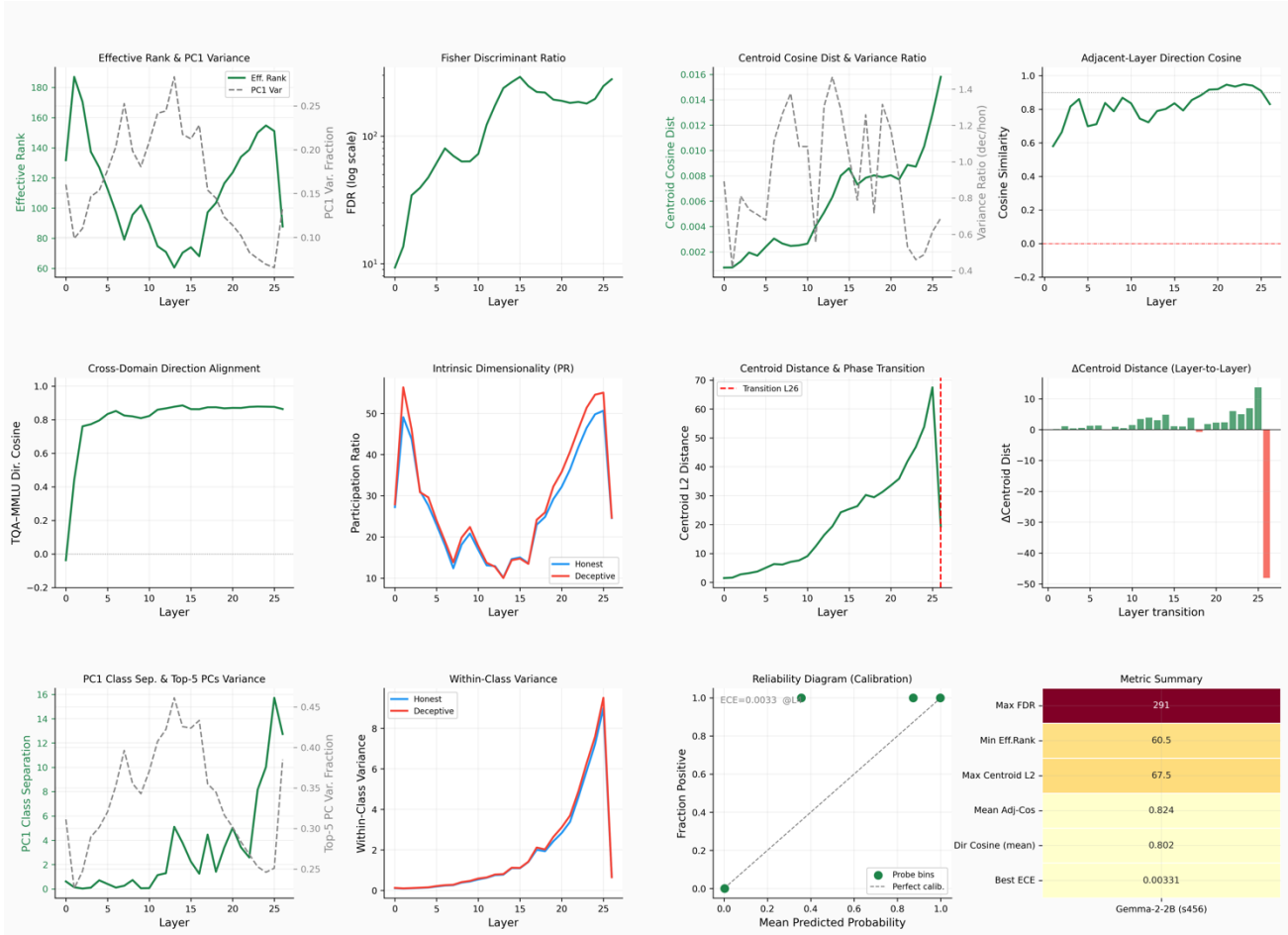


**Figure A5: Advanced Mechanistic Analysis (Gemma-2-2B, Seed 456)**

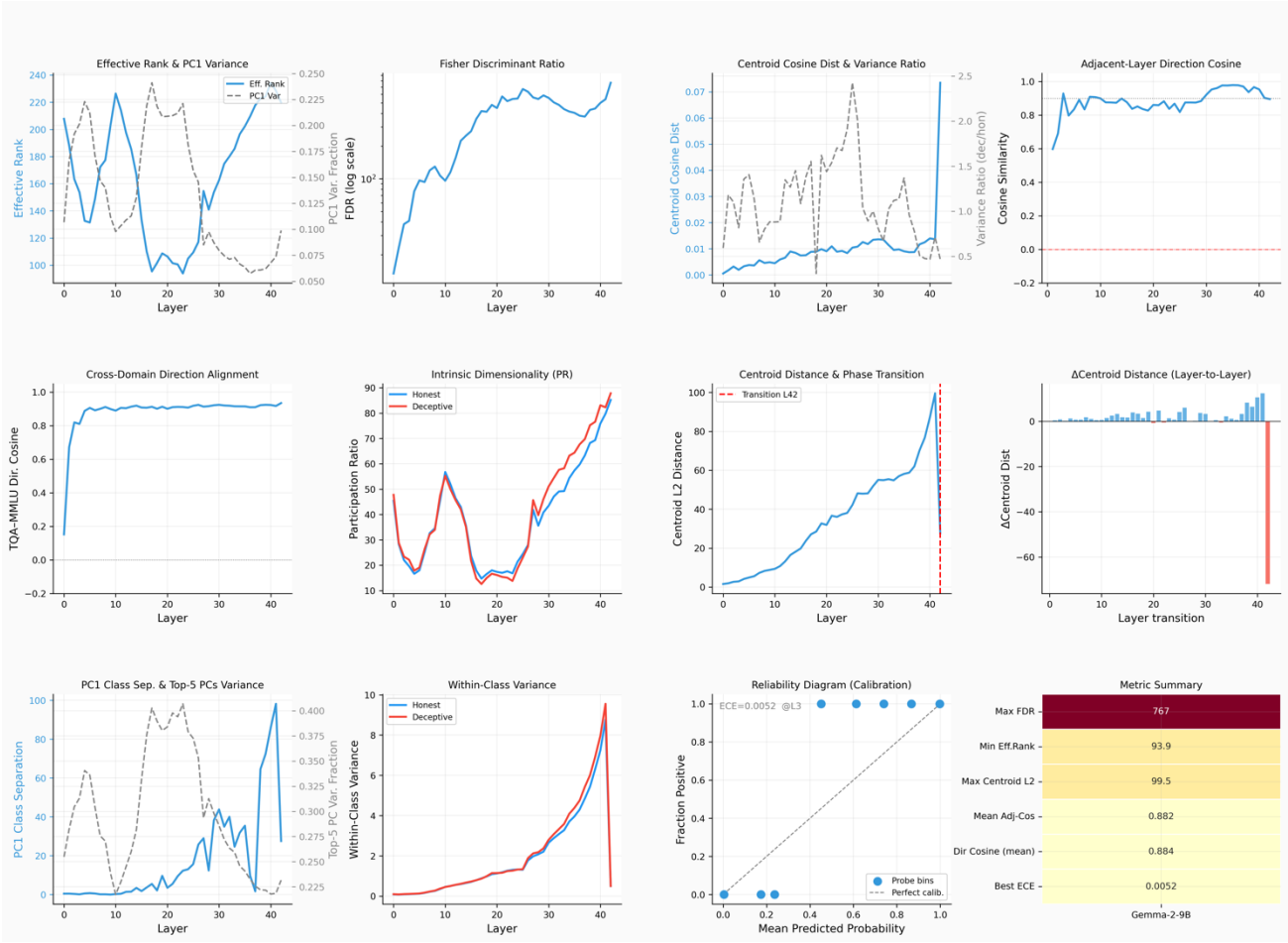


**Figure A2: Advanced Mechanistic Analysis (Gemma-2-9B)**

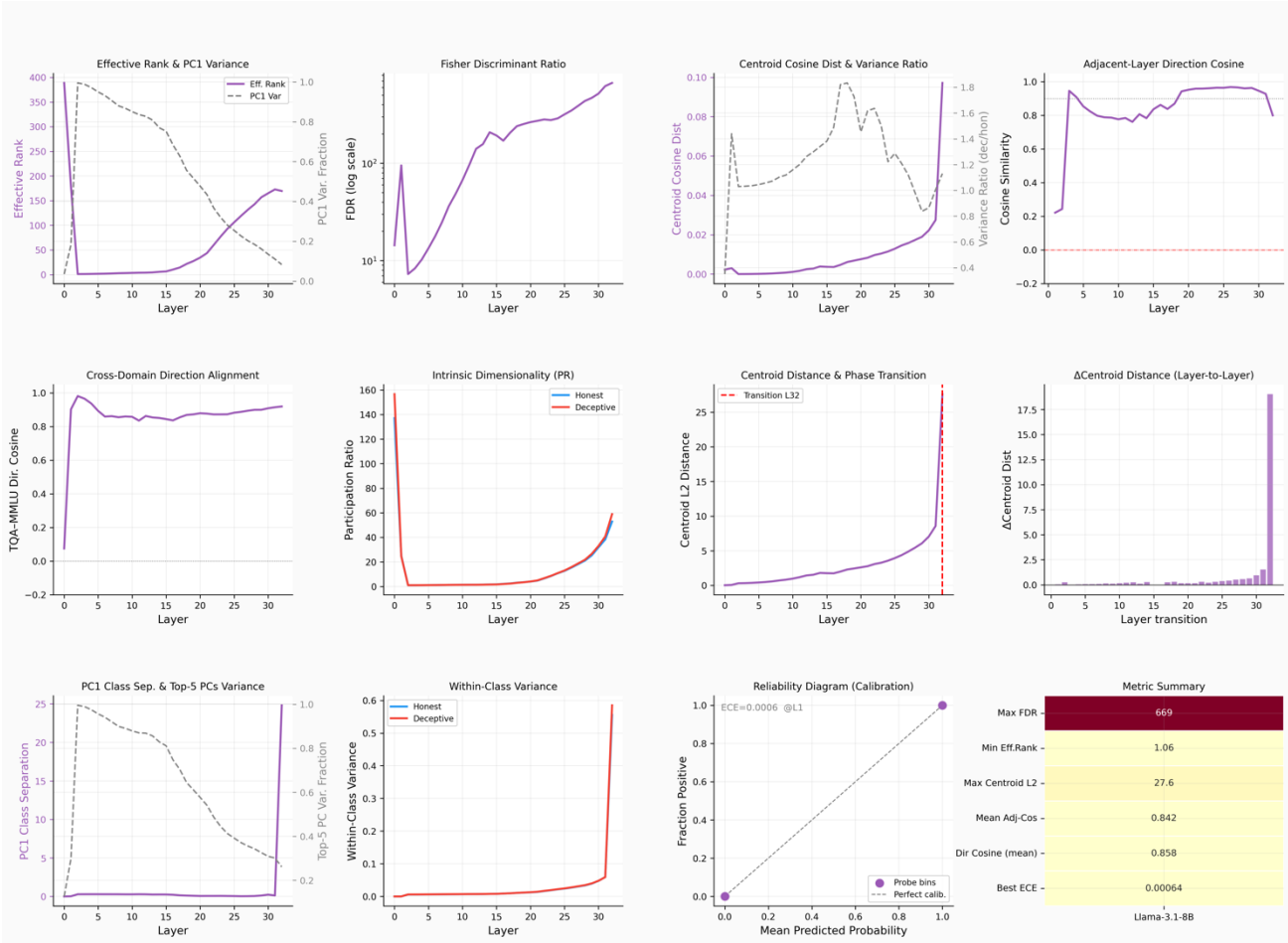


**Figure A6: Advanced Mechanistic Analysis (Llama-3.1-8B)**

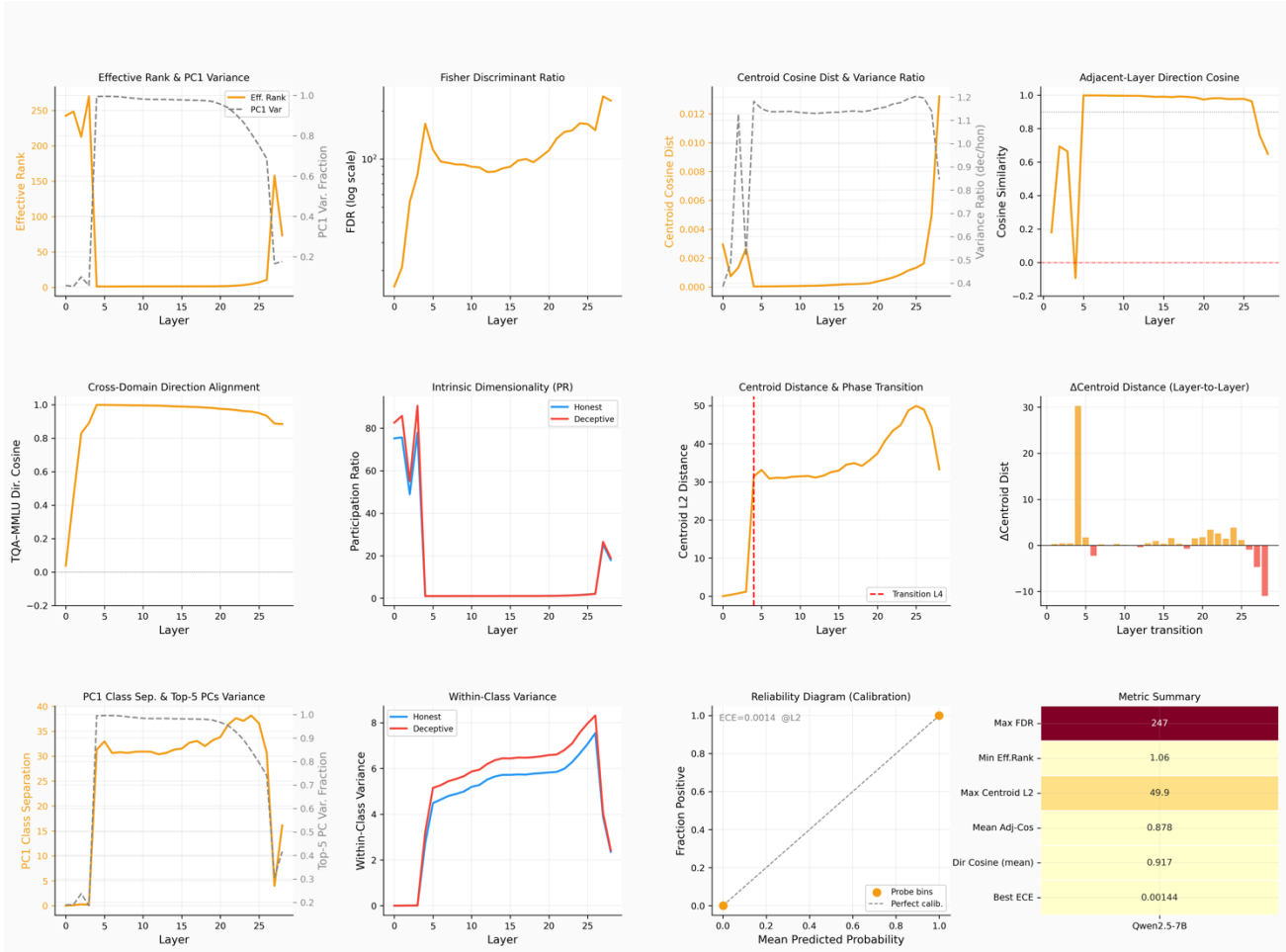


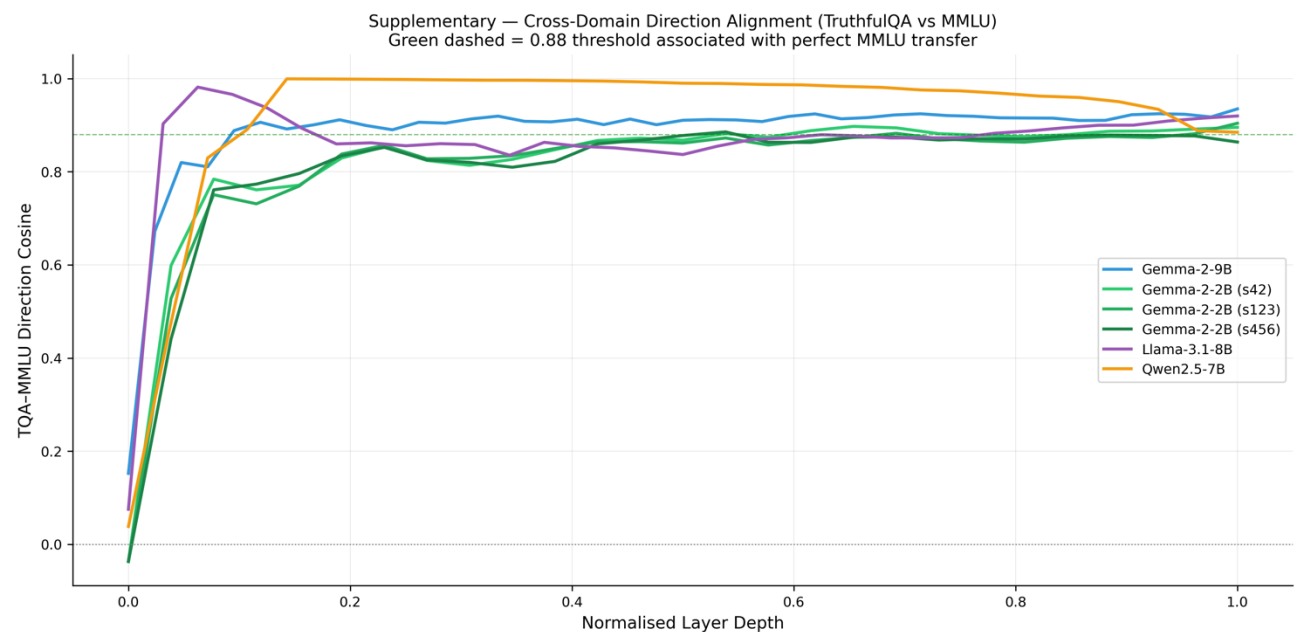
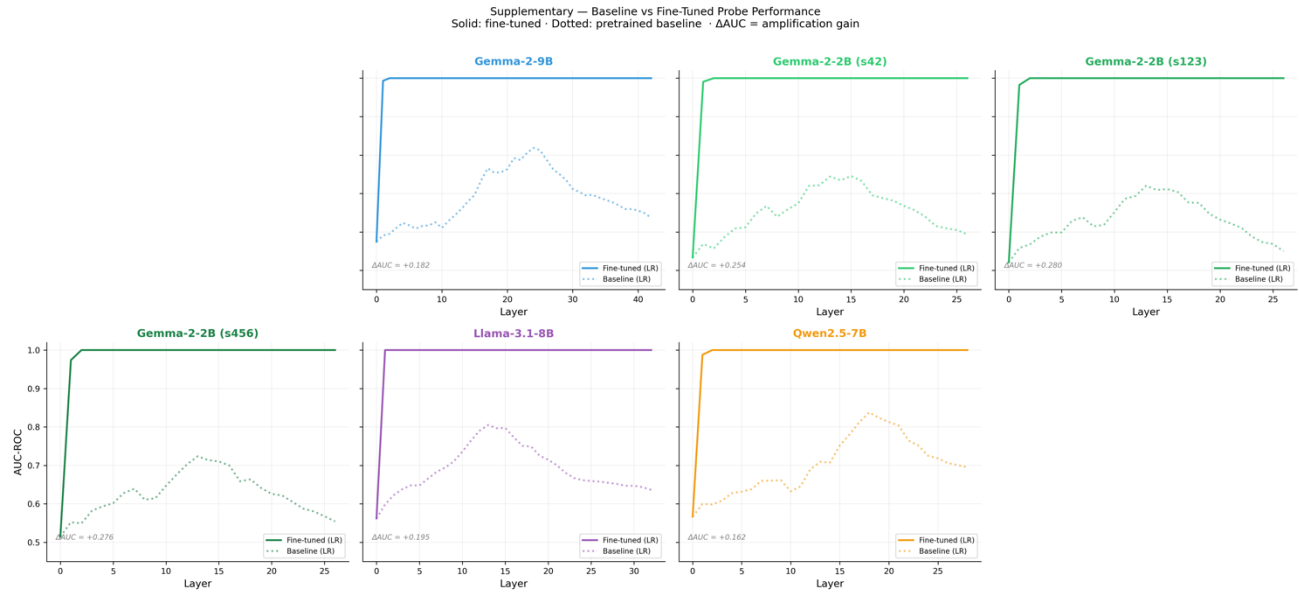
**Figure A7: Advanced Mechanistic Analysis (Qwen2.5-7B)**

**Figures A1–A7.** Advanced Mechanistic Analysis Panels (one per model). Each panel contains 12 subplots organized in a 3×4 grid: (Row 1) Effective Rank & PC1 Variance; Fisher Discriminant Ratio (log scale); Centroid Cosine Distance & Variance Ratio; Adjacent-Layer Cosine Similarity of Dishonesty Direction. (Row 2) TQA vs. MMLU Direction Alignment; Intrinsic Dimensionality (Participation Ratio); Centroid Distance Across Layers with Phase Transition;  $\Delta$ Centroid Distance (Layer-to-Layer). (Row 3) PC1 Class Separation & Top-5 PCs Variance; Within-Class Variance (Honest vs. Deceptive); Reliability Diagram (Calibration) at Best Layer; Metric Summary Heatmap.

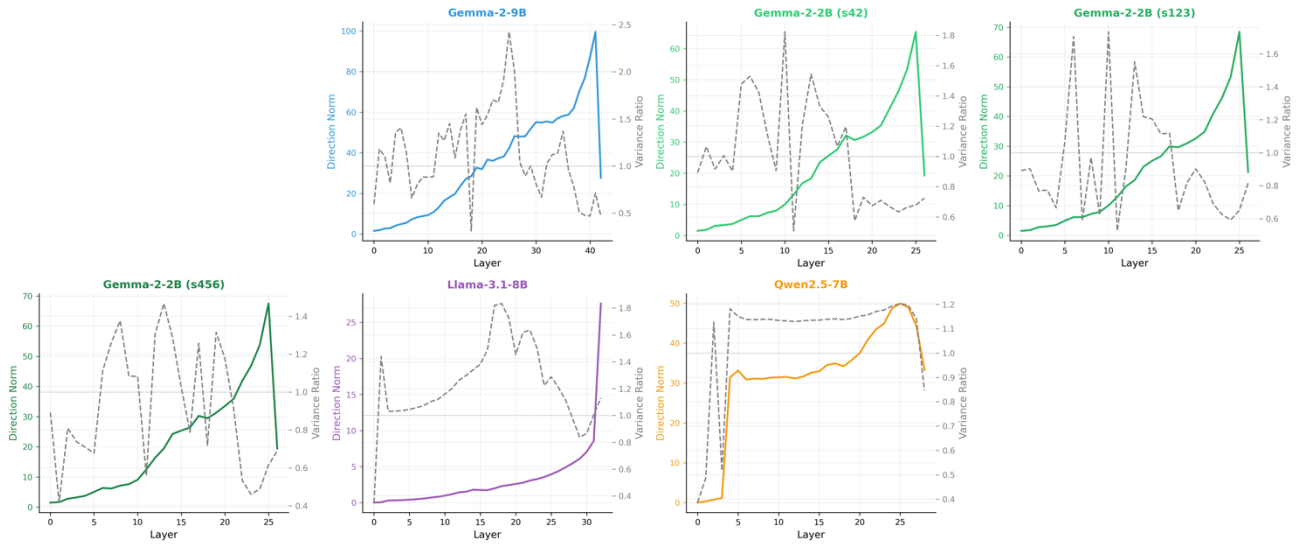
## Supplementary Material

## Advanced Mechanistic Analysis Figures (A1–A7)

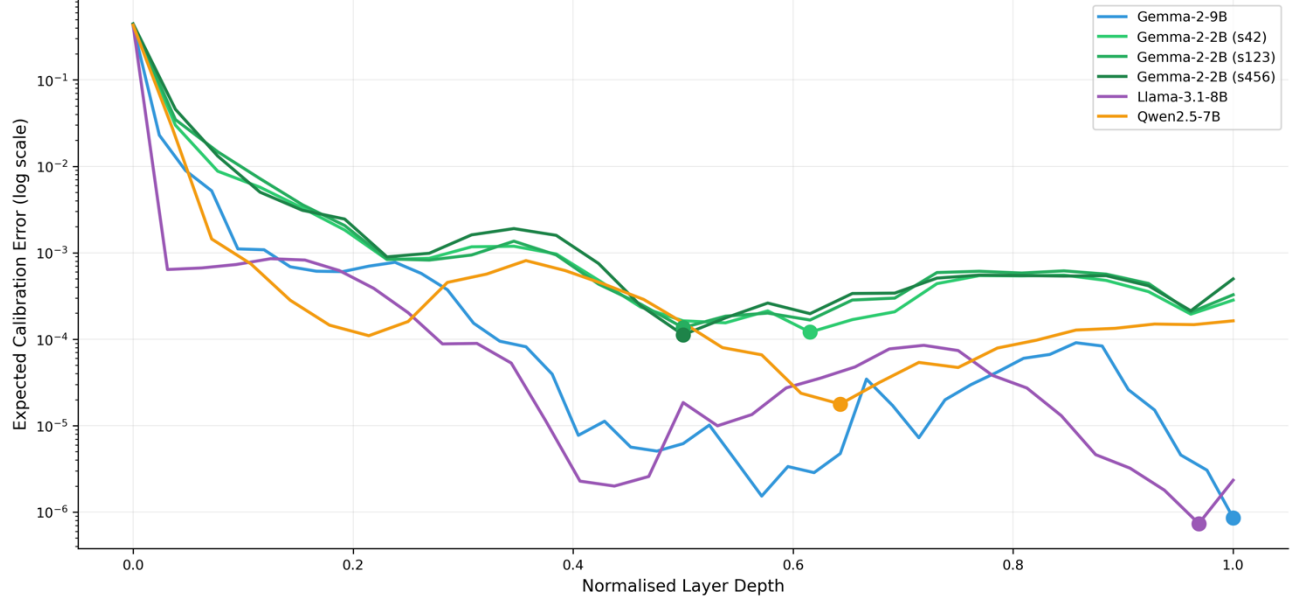
Full 12-subplot mechanistic analysis panels for all models: Pythia-1.4B (A1), Gemma-2-9B (A2), Gemma-2-2B seed 42 (A3), Gemma-2-2B seed 123 (A4), Gemma-2-2B seed 456 (A5), Llama-3.1-8B (A6), Qwen2.5-7B (A7). Each panel covers effective rank, Fisher Discriminant Ratio, centroid geometry, directional stability, cross-domain alignment, intrinsic dimensionality, calibration, and a summary heatmap.



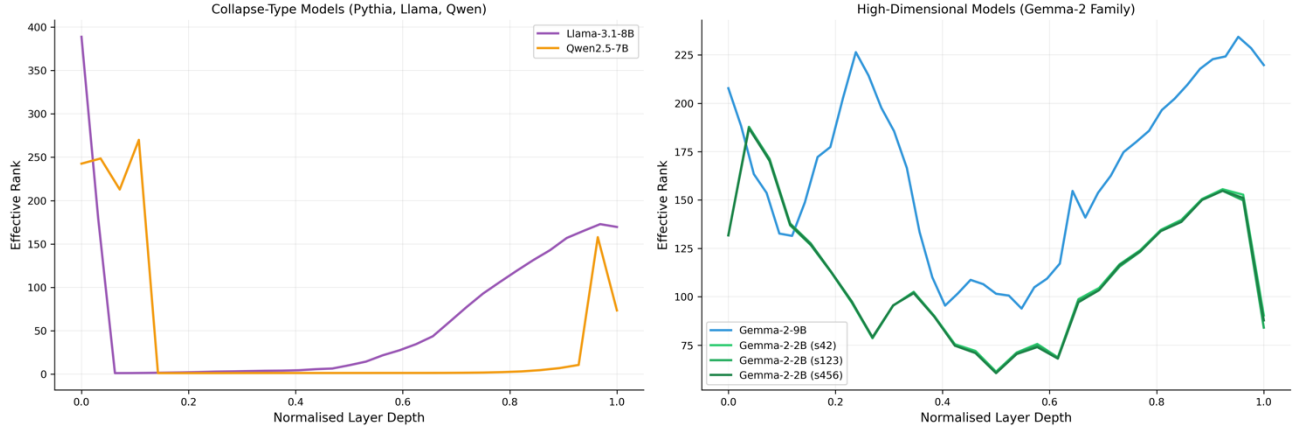
Supplementary — Dishonesty Direction Norm & Variance Ratio per Layer  
 Solid:  $|\text{direction}|$ ; Dashed:  $\text{Var}(\text{deceptive})/\text{Var}(\text{honest})$  along direction



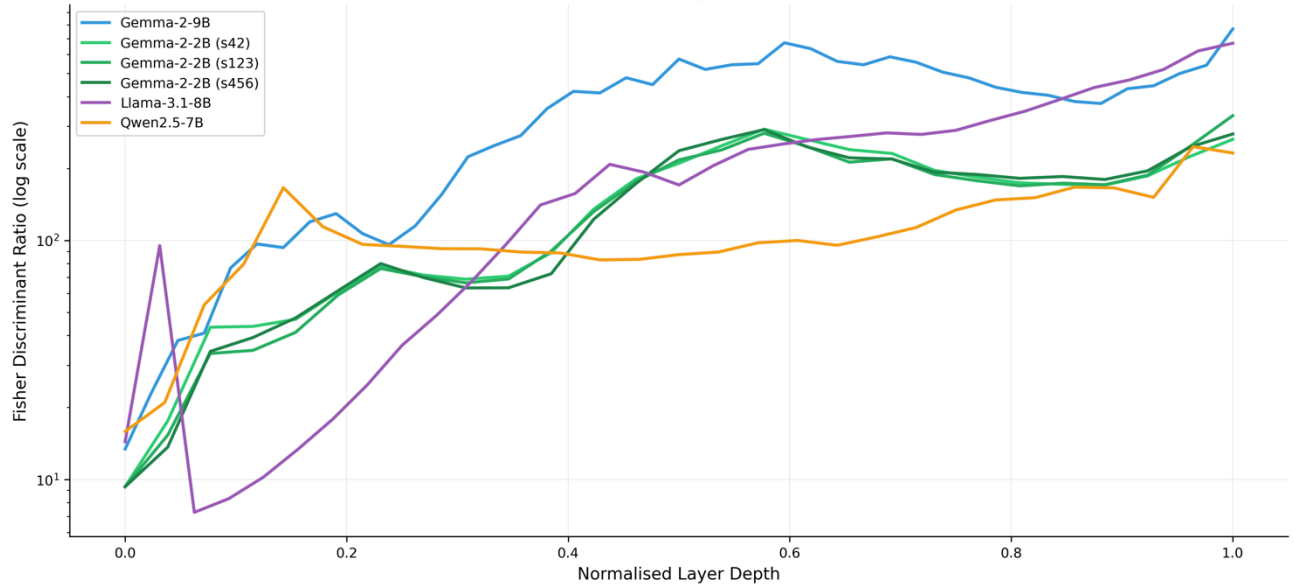
Supplementary — Layer-wise ECE (Logistic Regression Probe)



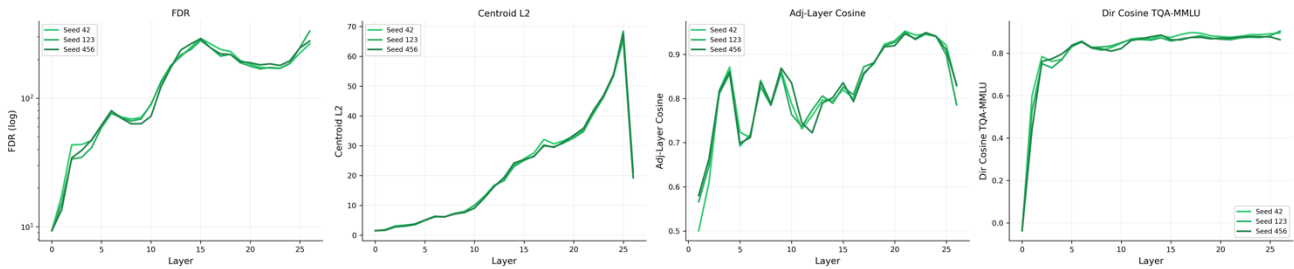
Supplementary — Effective Rank Bifurcation  
Collapse-type models hit near-rank-1 · Gemma-2 maintains high dimensionality



Supplementary — FDR Growth Across All Architectures  
(Monotonic increase from  $\approx 9.77$  [Pythia] to  $\approx 767$  [Gemma-2-9B])



Supplementary — Seed-Stratified Geometric Comparison: Gemma-2-2B (Seeds 42, 123, 456)



## Data and Code Availability

All probe training scripts and evaluation code are publicly available at <https://github.com/vzm1399/llm-dishonesty-representations>.

**Competing Interests:** None.

## Acknowledgments

This research was conducted as part of the AlgoVerse AI Research mentorship program. The author is profoundly grateful to the AlgoVerse team, especially and all mentors for their invaluable guidance, insightful feedback, and unwavering support throughout the project. Their expertise and dedication were instrumental in shaping the experimental design, mechanistic analyses, and overall quality of this work. This project would not have been possible without the resources, community, and rigorous research environment provided by AlgoVerse. The author also thanks the broader open-source AI community for the foundational models and tools that enabled this study.

## References

1. Hubinger E, Van Merwijk C, Mikulik V, Skalse J, Garrabrant S. Risks from learned optimization in advanced machine learning systems. arXiv preprint arXiv:190601820. 2019.
2. Hubinger E, Denison C, Mu J, Lambert M, Tong M, MacDiarmid M, et al. Sleeper agents: Training deceptive llms that persist through safety training. arXiv preprint arXiv:240105566. 2024.
3. Pacchiardi L, Chan A, Mindermann S, Moscovitz I, Pan A, Gal Y, et al., editors. How to catch an ai liar: Lie detection in black-box llms by asking unrelated questions. International Conference on Learning Representations; 2024.
4. Greenblatt R, Denison C, Wright B, Roger F, MacDiarmid M, Marks S, et al. Alignment faking in large language models. arXiv preprint arXiv:241214093. 2024.
5. Bai Y, Jones A, Ndousse K, Askell A, Chen A, DasSarma N, et al. Training a helpful and harmless assistant with reinforcement learning from human feedback. arXiv preprint arXiv:220405862. 2022.

6. Ouyang L, Wu J, Jiang X, Almeida D, Wainwright C, Mishkin P, et al. Training language models to follow instructions with human feedback. *Advances in neural information processing systems*. 2022;35:27730-44.
7. Burns C, Ye H, Klein D, Steinhardt J. Discovering latent knowledge in language models without supervision. *arXiv preprint arXiv:221203827*. 2022.
8. Marks S, Tegmark M. The geometry of truth: Emergent linear structure in large language model representations of true/false datasets. *arXiv preprint arXiv:231006824*. 2023.
9. Park K, Choe YJ, Veitch V. The linear representation hypothesis and the geometry of large language models. *arXiv preprint arXiv:231103658*. 2023.
10. Zou A, Phan L, Chen S, Campbell J, Guo P, Ren R, et al. Representation engineering: A top-down approach to ai transparency. *arXiv preprint arXiv:231001405*. 2023.
11. Hu EJ, Shen Y, Wallis P, Allen-Zhu Z, Li Y, Wang S, et al. Lora: Low-rank adaptation of large language models. *Iclr*. 2022;1(2):3.
12. Lin S, Hilton J, Evans O, editors. Truthfulqa: Measuring how models mimic human falsehoods. *Proceedings of the 60th annual meeting of the association for computational linguistics (volume 1: long papers)*; 2022.
13. Hendrycks D, Burns C, Basart S, Zou A, Mazeika M, Song D, et al. Measuring massive multitask language understanding. *arXiv preprint arXiv:200903300*. 2020.
14. MacDiarmid M, Maxwell T, Schiefer N, Mu J, Kaplan J, Duvenaud D, et al. Simple probes can catch sleeper agents, 2024. URL <https://www.anthropic.com/news/probes-catch-sleeper-agents>.
15. Meng K, Bau D, Andonian A, Belinkov Y. Locating and editing factual associations in gpt. *Advances in neural information processing systems*. 2022;35:17359-72.
16. Mitchell E, Lin C, Bosselut A, Finn C, Manning CD. Fast model editing at scale. *arXiv preprint arXiv:211011309*. 2021.
17. Malladi S, Gao T, Nichani E, Damian A, Lee JD, Chen D, et al. Fine-tuning language models with just forward passes. *Advances in Neural Information Processing Systems*. 2023;36:53038-75.
18. Goodfellow IJ, Shlens J, Szegedy C. Explaining and harnessing adversarial examples. *arXiv preprint arXiv:14126572*. 2014.
19. Madry A, Makelov A, Schmidt L, Tsipras D, Vladu A. Towards deep learning models resistant to adversarial attacks. *arXiv preprint arXiv:170606083*. 2017.
20. Guo C, Pleiss G, Sun Y, Weinberger KQ, editors. On calibration of modern neural networks. *International conference on machine learning*; 2017: PMLR.